CDF/ANAL/TOP/PUBLIC/10211
version 1.0
July 6, 2010

Measurement of $t\bar{t}$ Helicity Fractions and Spin Correlation Using Reconstructed Lepton+Jets Events

The CDF Collaboration[1]

Abstract

Standard model top pair production produces a characteristic spin correlation which can be modified by new production mechanisms such as Z' bosons or Kaluza-Klein gluons. In the standard model, top quarks decay weakly before any hadronization processes take effect, enabling top spin information to be transmitted to the top quark decay products. We report on the observation and measurement of the $t\bar{t}$ helicity fractions and spin correlation in 5.3 fb^{-1} of reconstructed lepton+jet data. In the helicity basis, we find the opposite helicity fraction $F_{OH} = 0.74 \pm 0.24(\text{stat}) \pm 0.11(\text{syst})$, and a spin correlation coefficient $\kappa_{helicity} = 0.48 \pm 0.48(\text{stat}) \pm 0.22(\text{syst})$. In the beam basis, we find the opposite spin fraction $F_{OS} = 0.86 \pm 0.32(\text{stat}) \pm 0.13(\text{syst})$, and a spin correlation coefficient $\kappa_{beam} = 0.72 \pm 0.64(\text{stat}) \pm 0.26(\text{syst})$.

[1] http://www-cdf.fnal.gov

1 Introduction

This note presents a measurement of the $t\bar{t}$ spin state using a 5.3fb^{-1} lepton+jets sample collected by the CDF detector at the Fermilab Tevatron. It is an update of a previous measurement performed using 4.3fb^{-1} [1]. In the standard model the top quark lifetime is shorter than the spin decoherence time, and the $t\bar{t}$ spin state at decay is mapped onto the V-A correlations in the final state. The $q\bar{q}$ annihilations that comprise $\sim 85\%$ of our sample should show the dominance of the $S = 1$ gluon annihilation channel. New physics could change this, and models of new physics appeal to the spin-correlation for signal identification and discrimination [2, 3].

Choosing the direction of the top quark momentum as our spin quantization axis (the "helicity basis"), the $t\bar{t}$ spin can be described by four independent helicity states $\bar{t}_L t_R, \bar{t}_R t_L, \bar{t}_L t_L, \bar{t}_R t_R$. In the $t\bar{t}$ rest frame the quarks move back-to-back and the same spin ($S = 1$) states are those with opposite helicity $\bar{t}_L t_R, \bar{t}_R t_L$. At threshold the opposite helicity fraction is 67%; at very high momentum helicity is conserved and this fraction rises to 100 [4, 5]. Integrating over all top momenta according to the pdf's and adding the small ($\sim 15\%$) $S = 0$ contribution from gg, we expect to find an opposite helicity fraction

$$F_{OH} = \frac{\sigma(\bar{t}_R t_L) + \sigma(\bar{t}_L t_R)}{\sigma(\bar{t}_R t_R + \bar{t}_L t_L + \bar{t}_R t_L + \bar{t}_L t_R)} = \frac{N_o}{N_o + N_s} \approx 0.70. \quad (1)$$

where N_o and N_s are the numbers of opposite and same helicity events [4].

This analysis measures F_{OH} in the helicity basis by fitting the helicity angle bilinears $\cos(\theta_l)\cos(\theta_d)$ and $\cos(\theta_b)\cos(\theta_d)$ to the sum of template distributions for the four $t\bar{t}$ helicity eigenstates. Since CP conservation implies $\sigma(\bar{t}_R t_R) = \sigma(\bar{t}_L t_L)$, the same helicity (SH) template shape is symmetric sum of $\sigma(\bar{t}_R t_R) + \sigma(\bar{t}_L t_L)$. Since P conservation implies $\sigma(\bar{t}_R t_L) = \sigma(\bar{t}_L t_R)$, the opposite helicity (OH) template shape is the symmetric sum of $\sigma(\bar{t}_R t_R) + \sigma(\bar{t}_L t_L)$. The helicity angle bilinears are fit to the sum of the OH and SH templates and we measure the opposite helicity fraction F_{OH} as above.

Additionally, in this analysis, we also perform a measurement in the beamline basis, where the spin quantization axis is chosen to be the direction of the beamline. We measure the fraction of top quarks with opposite spin,F_{OS} , in this basis in the same way as we measure F_{OH} in the helicity basis.

The $t\bar{t}$ spin state is often discussed in terms of the spin-correlation parameter

$$\kappa = \frac{[\sigma(\bar{t}_R t_L) + \sigma(\bar{t}_L t_R)] - [\sigma(\bar{t}_R t_R) + \sigma(\bar{t}_L t_L)]}{\sigma(\bar{t}_R t_R) + \sigma(\bar{t}_L t_L) + \sigma(\bar{t}_R t_L) + \sigma(\bar{t}_L t_R)} = \frac{N_o - N_s}{N_o + N_s}. \quad (2)$$

which is simply related to the opposite spin fraction $F_{OS} = \frac{1}{2}(1 + \kappa)$. For uncorrelated spins, $\kappa = 0$, and $f_o = 0.5$. At next-to-leading-order, we expect to find $\kappa = 0.35$ in the helicity basis and $\kappa = 0.77$ in the beamline basis [6]. In [1], the measurement yielded $F_{OH} = 0.80 \pm 0.25 \pm 0.08$, corresponding to $\kappa = 0.60 \pm 0.50 \pm 0.16$. A recent and elegant CDF measurement [7] uses kinematic reconstruction in the dilepton sample to find the lepton and b-quark helicity angles in the off-diagonal basis [5] and then fits the

2D distributions of these angles to the expected functional form. In 2.8 fb^{-1} of data this yields $\kappa = 0.32^{+0.55}_{-0.78}$.

2 Data Sample and Event Selection

We analyze a 5.3 fb^{-1} dataset in the lepton+jets channel, consisting of a total of 725 events. The event selection requires one central lepton with large transverse momentum, missing transverse energy of at least 20 GeV, and 4 or more tight jets, at least one of which must be tagged as a b jet. The background is calculated using a combination of Monte Carlo samples and data samples, with a predicted total of 110 $\pm$ 19 background events. For details of the event selection and background calculation, see [8].

Our analysis revolves around the correlation of the decay angles of the lepton and the down and bottom quarks coming from the hadronically decaying top. These angles carry information about the spin of the parent top quark. In the helicity basis, the decay angle is defined as the angle between the decay product momentum (in the top rest frame) and the top momentum (in the $t\bar{t}$ rest frame), while in the beam basis the deday angle is defined to be the angle between the decay product momentum (in the top rest frame) and the beamline direction (in the $t\bar{t}$ rest frame). We are able to determine the top and $t\bar{t}$ rest frames by using a χ^2 based kinematic fitter where the top mass is contrained to 172.5 GeV. We impose a cut on the quality of this kinematic reconstruction, requiring $\chi^2 < 9.0$ in order for events to pass our selection. This reduces our dataset from 1260 events that pass the basic selection to the 725 events that we use in the analysis. Additionally, this cut reduces the background expectation from 283 events to 110 events, increasing our signal to background ratio from 3.5:1 to 5.6:1. In order to validate our event selection, kinematic reconstruction, and background model, we look at the cosines of these three helicity basis angles in Figures 1 through 3 and the cosines of the beamline basis angles in Figures 4 through 6. In these figures, our selected data sample is compared to the sum of our background model and a $t\bar{t}$ signal sample created using PYTHIA, which does not contain a spin correlation effect. These figures include the results of a Kolmogorov-Smirnov (KS) test comparing the data to the model prediction, and we see good agreement.

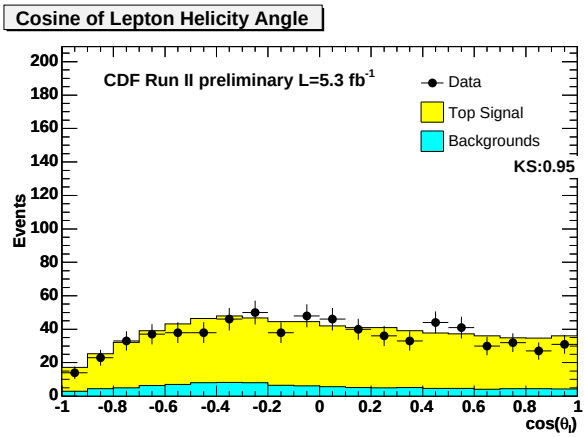

Figure 1: Helicity basis distribution of $cos(\theta_l)$ variable in data compared to the sum of our background model (light blue) and a PYTHIA signal model (yellow).

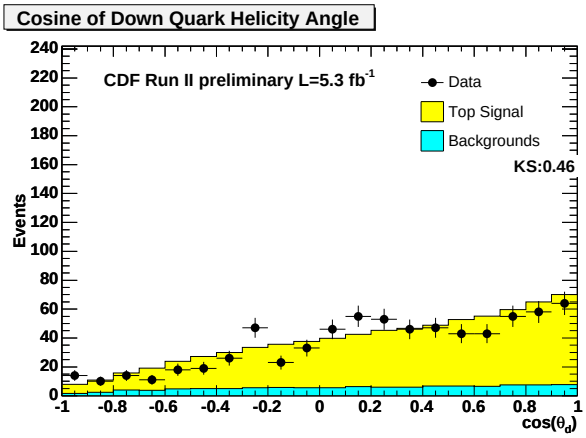

Figure 2: Helicity basis distribution of $cos(\theta_d)$ variable in data compared to the sum of our background model (light blue) and a PYTHIA signal model (yellow).

We validate our background model by comparing the predicted shape to the background rich sample with no b-tags (the "anti-tag" sample). Figure 7 shows the product $\cos(\theta_l)\cos(\theta_d)$ for the anti-tag sample in the helicity basis, compared to our background model summed with the small expected contribution from $t\bar{t}$ events, modeled by PYTHIA, while Figure 8 shows the same plot in the beamline basis. The model is seen to be a good reproduction of the data.

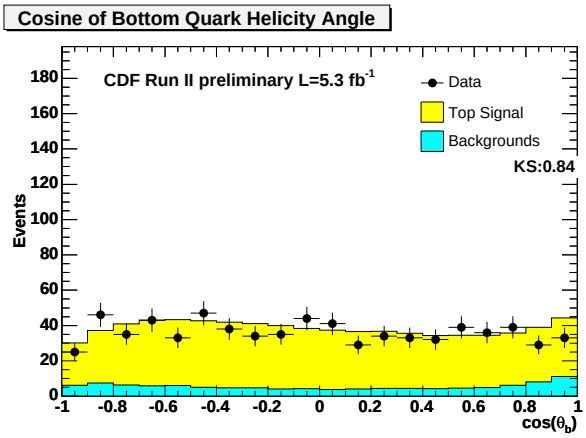

Figure 3: Helicity basis distribution of $cos(\theta_b)$ variable in data compared to the sum of our background model (light blue) and a PYTHIA signal model (yellow).

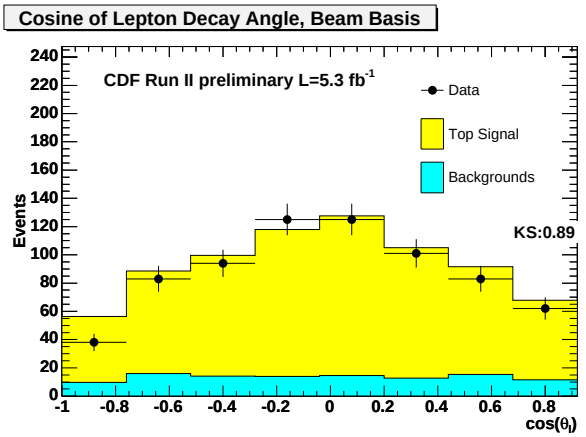

Figure 4: Beamline basis distribution of $cos(\theta_l)$ variable in data compared to the sum of our background model (light blue) and a PYTHIA signal model (yellow).

3 Template Creation and Measurement Method

3.1 Same Helicity and Opposite Helicity Templates

We use a binned likelihood template fit which requires same helicity and opposite helicity templates in order to perform a fit to the data. In the helicity basis, these templates were created using a modified version of the HERWIG Monte Carlo generator, while in the beamline basis they were created by reweighted a sample created by the PYTHIA Monte Carlo generator.

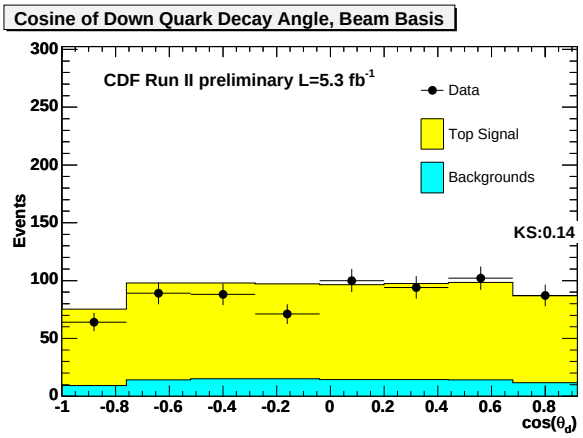

Figure 5: Beamline basis distribution of $cos(\theta_d)$ variable in data compared to the sum of our background model (light blue) and a PYTHIA signal model (yellow).

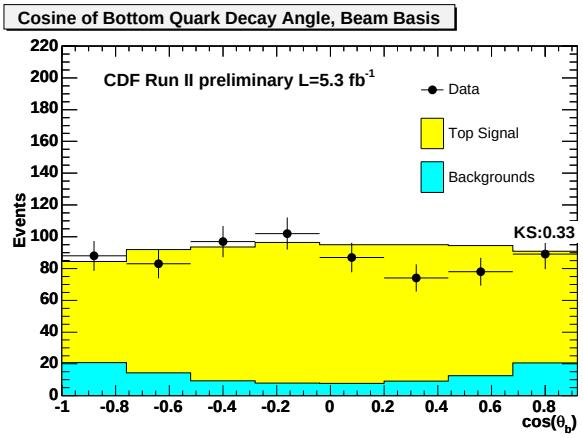

Figure 6: Beamline basis distribution of $cos(\theta_b)$ variable in data compared to the sum of our background model (light blue) and a PYTHIA signal model (yellow).

3.1.1 Helicity Basis Templates

In top quark decays, the angular distributions of the top decay products determined by the helicity of the parent top quark via Equation 3

$$f(\cos(\theta_i)) = \frac{1}{2}(1 \pm A_i \cos(\theta_i)) \tag{3}$$

where the positive sign is for right-handed top quarks and the negative sign refers to left-handed top quarks (the signs are reversed for antitop decays). The correlation coefficient A_i varies for each decay product, being equal to +1.0 for the charged lepton or down quark, -0.41 for the bottom quark, and -0.31 for the neutrino or up quark [5].

We created our templates by modifying the HERWIG source code to implement this angular distribution for the charged lepton or down type quark, and then allowing

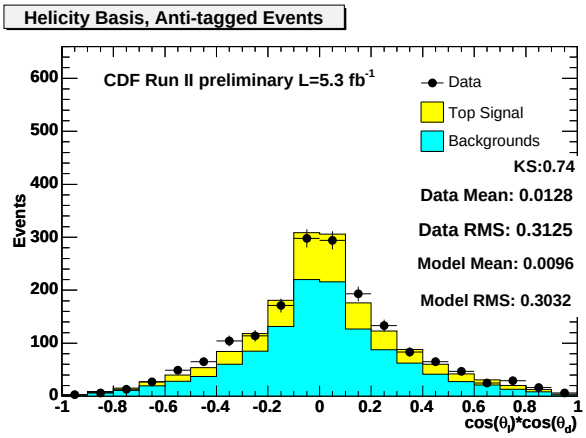

Figure 7: Helicity basis distribution of $\cos(\theta_l)\cos(\theta_d)$ variable in anti-tagged data sample compared to the sum of our background model (light blue) and a PYTHIA signal model (yellow).

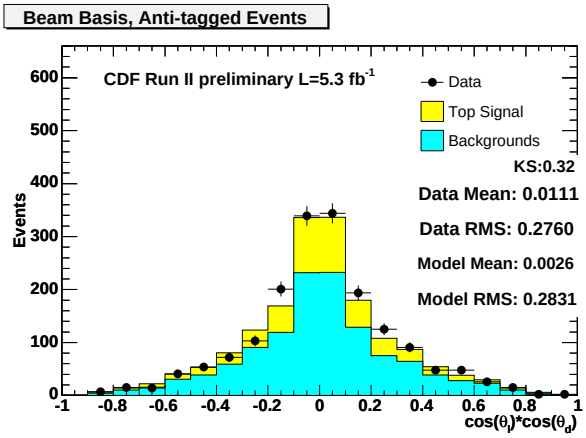

Figure 8: Beamline basis distribution of $\cos(\theta_l)\cos(\theta_d)$ variable in anti-tagged data sample compared to the sum of our background model (light blue) and a PYTHIA signal model (yellow).

the internal HERWIG machinery to propagate the appropriate angular distributions to the other decay products. Using this modified HERWIG, we then created four different simulated Monte Carlo samples, corresponding to the four possible top pair helicity states, $\bar{t}_L t_R, \bar{t}_R t_L, \bar{t}_L t_L, \bar{t}_R t_R$. Figures 9 through 11 show the truth-level angular distributions for the top quark decay products for these four helicity samples, while Figures 12 through 14 show the same for the antitop quark decay products. In all cases, the expecte slopes are observed.

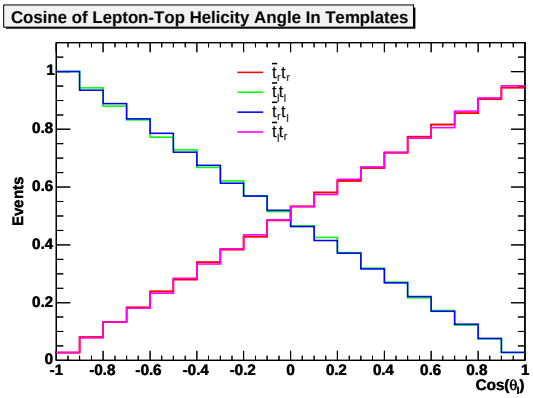

Figure 9: Distribution of $cos(\theta_l)$ variable in top quark decays at truth level for our four samples representing the four different top pair helicity states. The samples show the expected slopes of +1 for right-handed tops and -1 for left-handed tops.

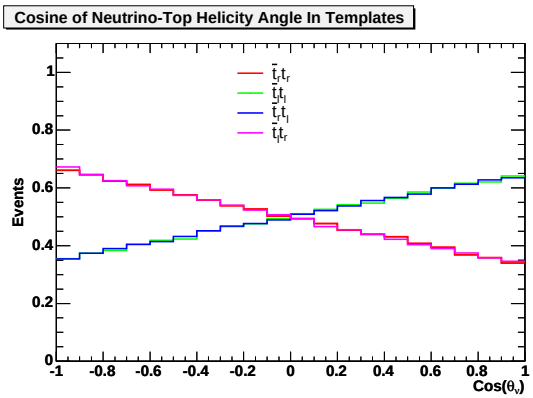

Figure 10: Distribution of $cos(\theta_\nu)$ variable in top quark decays at truth level for our four samples representing the four different top pair helicity states. The samples show the expected slopes of -0.31 for right-handed tops and +0.31 for left-handed tops.

With the simulated samples prepared for the four different top pair helicity states, templates were created by combining the $\bar{t}_L t_R$ and $\bar{t}_R t_L$ samples in equal ratios according to parity conservation to form an opposite helicity sample and combining the $\bar{t}_L t_L$ and $\bar{t}_R t_R$ samples in equal ratios according to CP conservation to form a same helicity sample. To show the effect of the top quark helicity states on the distributions of interest in this analysis, Figure 15 shows the variable $\cos(\theta_l)\cos(\theta_d)$, comparing the distribution at truth level in HERWIG without spin correlations to the same and opposite helicity templates respectively.

Figure 15 assumes that the down quark can be identified 100% efficienctly, but one of the difficulties of this analysis is that this is not the case. In order to choose the down quark, we use the precription described in [5]: the jet closest to the b jet in the W rest frame will be the d jet approximately 60% of the time. Figure 16 again

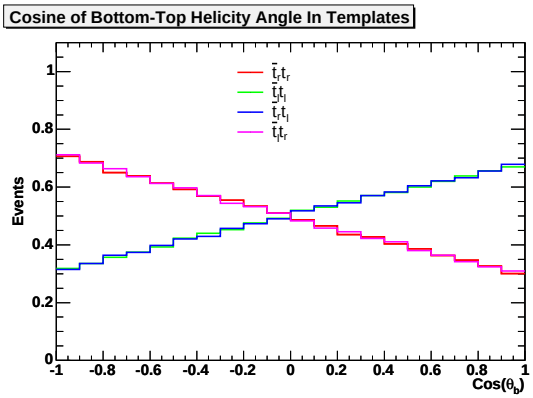

Figure 11: Distribution of $cos(\theta_b)$ variable in top quark decays at truth level for our four samples representing the four different top pair helicity states. The samples show the expected slopes of -0.41 for right-handed tops and +0.41 for left-handed tops.

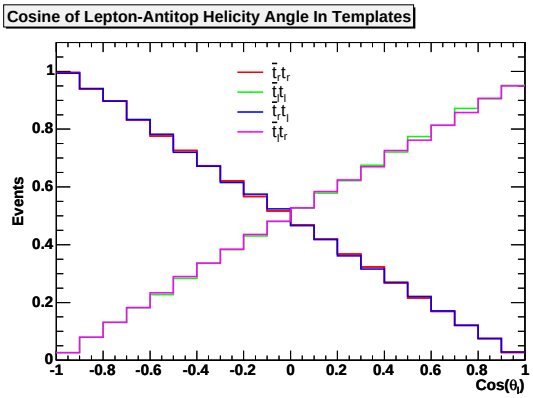

Figure 12: Distribution of $cos(\theta_l)$ variable in antitop quark decays at truth level for our four samples representing the four different top pair helicity states. The samples show the expected slopes of -1 for right-handed antitops and +1 for left-handed antitops.

shows $\cos(\theta_l)\cos(\theta_d)$ at truth level, comparing HERWIG without spin correlations to our same and opposite helicity templates, but in these figures the down quark is chosen using this prescription. This probabilistic choice reduces the difference between our templates and uncorrelated HERWIG, but a significant effect is still present.

3.1.2 Beamline Basis Templates

In the beamline basis, we create our template samples by reweighting a PYTHIA sample, which starts out with no spin correlations, according to Equation 3. This is, in effect, the same procedure used for our helicity basis templates, but here it is imposed after event generation rather than before. The resulting templates are show in Figure 17, while Figure 18 shows these templates after our algorithm for choosing the down quark has been applied.

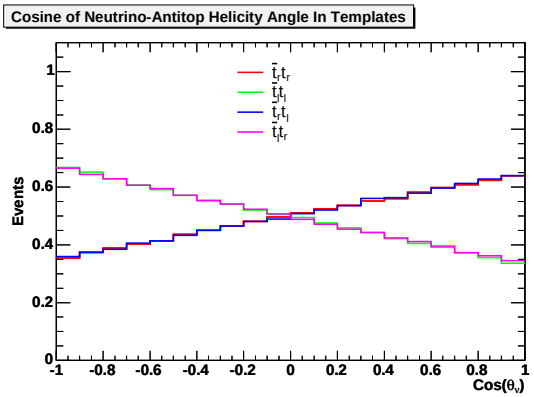

Figure 13: Distribution of $cos(\theta_\nu)$ variable in antitop quark decays at truth level for our four samples representing the four different top pair helicity states. The samples show the expected slopes of +0.31 for right-handed antitops and -0.31 for left-handed antitops.

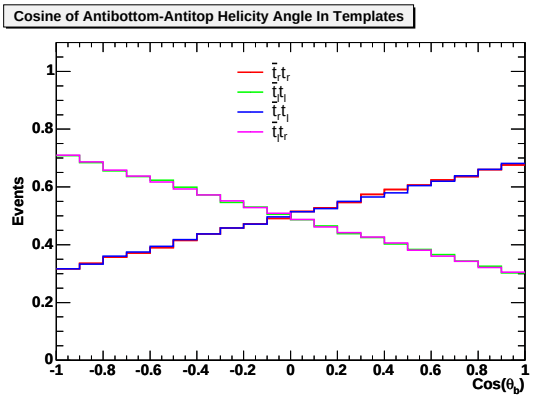

Figure 14: Distribution of $cos(\theta_b)$ variable in antitop quark decays at truth level for our four samples representing the four different top pair helicity states. The samples show the expected slopes of +0.41 for right-handed antitops and -0.41 for left-handed antitops.

3.2 Measurement Method

With the templates created, we can now use them in performing our fit. Our fitting method is a binned likelihood fit to the data, using three separate templates - the same spin template, the opposite spin template, and the background template. The background template was discussed in Section 2. Figure 19 shows the various components that go into this background template, and their relative sizes, for the $\cos(\theta_l)\cos(\theta_d)$ distribution in the helicity basis, while Figure 20 shows the same for the beamline basis.

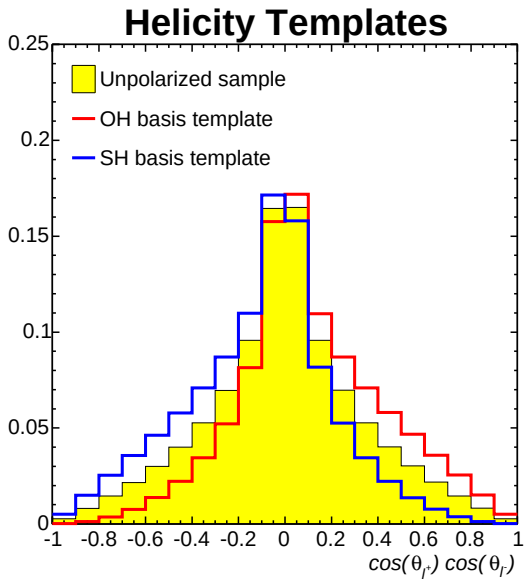

Figure 15: Truth distribution of $\cos(\theta_l)\cos(\theta_d)$ variable in our helicity basis template samples compared to HERWIG with no spin correlations. The d quark in this plot is always identified correctly.

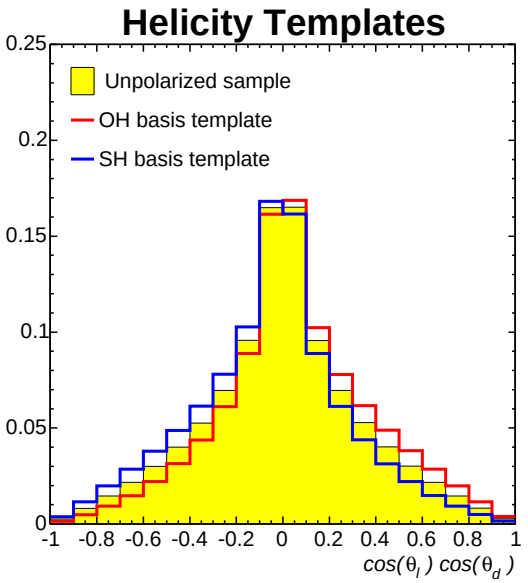

Figure 16: Truth distribution of $\cos(\theta_l)\cos(\theta_d)$ variable in our helicity basis template samples compared to HERWIG with no spin correlations. The d quark is chosen probabilistically to be the jet closest to the b jet in the W rest frame.

We consider two separate decay angle bilinears in our fit, $\cos(\theta_l)\cos(\theta_d)$ and $\cos(\theta_l)\cos(\theta_b)$. Two 1-dimensional likelihood fits could be performed using these two variables, but pseudoexperiments show that there is a significant gain in sensitivity when the two variables are combined into a single 2-dimensional fit, so this is the chosen method for our measurement. When performing the fit, the background normalization is Gaussian-constrained to the predicted value, but the same helicity fraction F_{SH} and opposite helicity fraction F_{OH} are allow to float freely. We do not require that F_{SH} and F_{OH} be constrained to physical values between 0 and 1, but we do require $F_{SH} + F_{OH} = 1$. In the helicity basis, we have an expected statistical uncertainty on F_{OH} of 0.22, while in the beamline basis the expected uncertainty on F_{OS} is 0.31. The change in uncertainty is an acceptance effect caused by differences in the number of sensitive events passing our selection in each basis.

4 Systematic Uncertainties

There are a number of systematic effects that contribute to our uncertainty which need to be taken into account. These include uncertainties in the background size and shape, uncertainties in the exact detector response, and uncertainties in the underlying

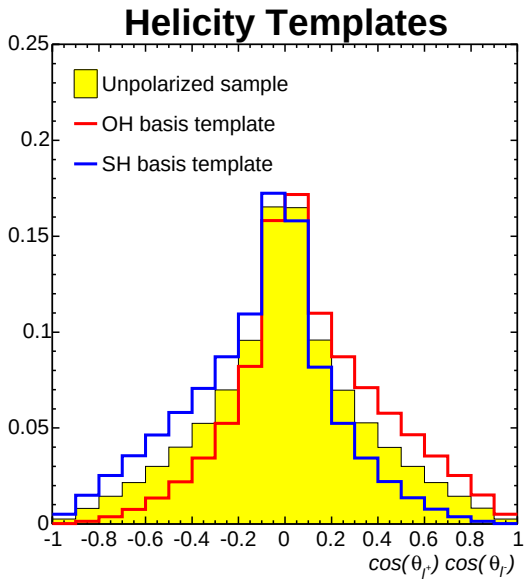

Figure 17: Truth distribution of $\cos(\theta_l)\cos(\theta_d)$ variable in our beamline basis template samples compared to HERWIG with no spin correlations. The d quark in this plot is always identified correctly.

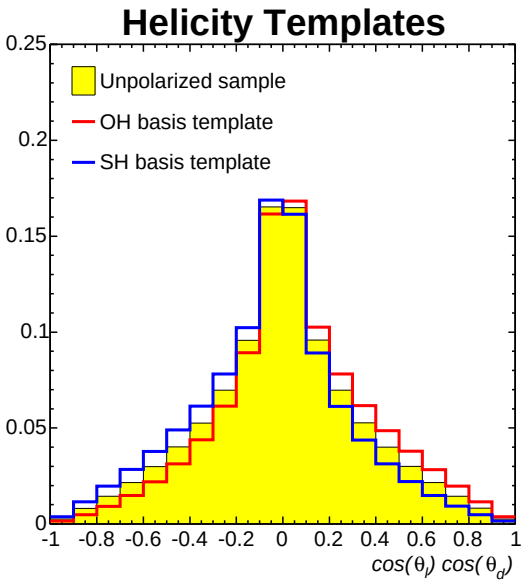

Figure 18: Truth distribution of $\cos(\theta_l)\cos(\theta_d)$ variable in our beamline basis template samples compared to HERWIG with no spin correlations. The d quark is chosen probabilistically to be the jet closest to the b jet in the W rest frame.

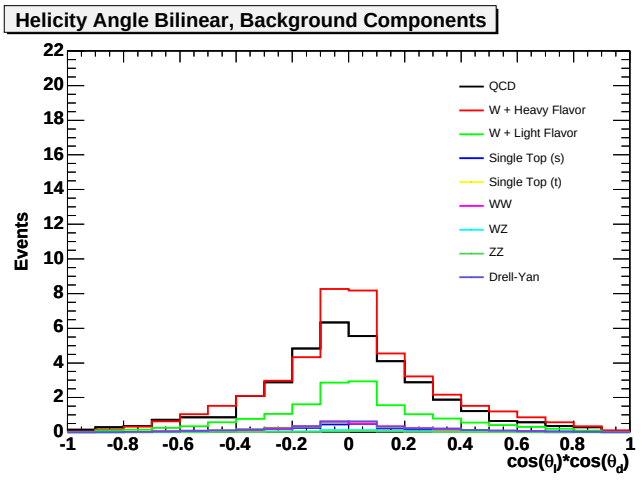

Figure 19: Helicity basis distribution of the $\cos(\theta_l)\cos(\theta_d)$ variable for the various components of our background template. The largest component of our background model consists of W + heavy flavor jet events.

structure of the colliding particles. Each of these uncertainties is handled its own unique way, but all follow the same general procedure. We start with a template consisting

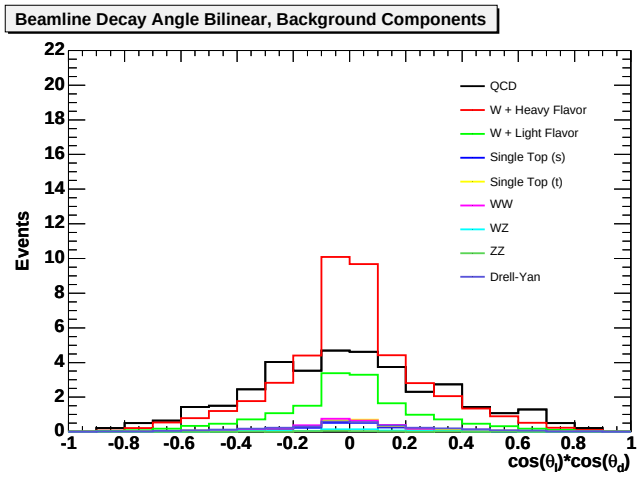

Figure 20: Beamline basis distribution of the $\cos(\theta_l)\cos(\theta_d)$ variable for the various components of our background template. The largest component of our background model consists of W + heavy flavor jet events.

of a nominal background and signal model, and then replace either the background or signal model with a model where the appropriate systematic effect has been varied. Our fit is then performed using this new template, and the result compared to the nominal result in order to determine the systematic uncertainty. These uncertainties are calculated separately in the helicity basis and the beam basis. In both cases, the largest uncertainty is the "MC Generator" uncertainty, resulting from the fact that when performing our measurement in certain simulated samples with known values for the opposite spin fraction, there are small deviations from the expected result. Although this is our largest systematic uncertainty, it is still small compared to our statistical uncertainty. The resulting uncertainties from these studies are contained in Table 1 for the helicity basis and Table 2 for the beamline basis.

Systematic	Uncertainty
MC Generator	0.1000
JES	0.0274
Background Shape	0.0193
ISR/FSR	0.0090
Color Reconnection	0.0077
Parton Shower	0.0061
PDF	0.0034
Background Size	0.0003
Total Uncertainty	0.1064

Table 1: Summary of Helicity Basis Systematic Uncertainties

Systematic	Uncertainty
MC Generator	0.1000
Background Shape	0.0601
Color Reconnection	0.0472
ISR/FSR	0.0446
PDF	0.0105
JES	0.0087
Parton Shower	0.0008
Background Size	0.0008
Total Uncertainty	0.1342

Table 2: Summary of Beamline Basis Systematic Uncertainties

5 Results

With our fitting procedure established and all systematics uncertainties calculated, the final result of our 2-dimensional fit of $\cos(\theta_l)\cos(\theta_d)$ vs. $\cos(\theta_l)\cos(\theta_b)$ in data corresponding to an integrated luminosity of 5.3fb^{-1} in the helicity basis returns an oppsite helicity fraction of

$$F_{OH} = 0.74 \pm 0.24_{\text{stat}} \pm 0.11_{\text{syst}} \quad .$$

Converting this to the spin correlation coefficient using $\kappa = 2 * f_o - 1$ yields

$$\kappa_{helicity} = 0.48 \pm 0.48_{\text{stat}} \pm 0.22_{\text{syst}} \quad .$$

In the beamline basis, we find an opposite spin fraction of

$$F_{OS} = 0.86 \pm 0.32_{\text{stat}} \pm 0.13_{\text{syst}} \quad .$$

which can be converted in to a correlation coefficient of

$$\kappa_{beam} = 0.72 \pm 0.64_{\text{stat}} \pm 0.26_{\text{syst}} \quad .$$

Figures 21 and 22 show the helicity basis 1-dimensional distributions for $\cos(\theta_l)\cos(\theta_d)$ and $\cos(\theta_l)\cos(\theta_b)$ respectively, where our data is compared to the sum of the background model, same helicity model, and opposite helicity model, with the normalizations determined by the result of our fit for F_{OH}. Figures 23 and 24 show the same thing in the beamline basis.

Acknowledgments

We thank the Fermilab staff and the technical staffs of the participating institutions for their vital contributions. This work was supported by the U.S. Department of Energy

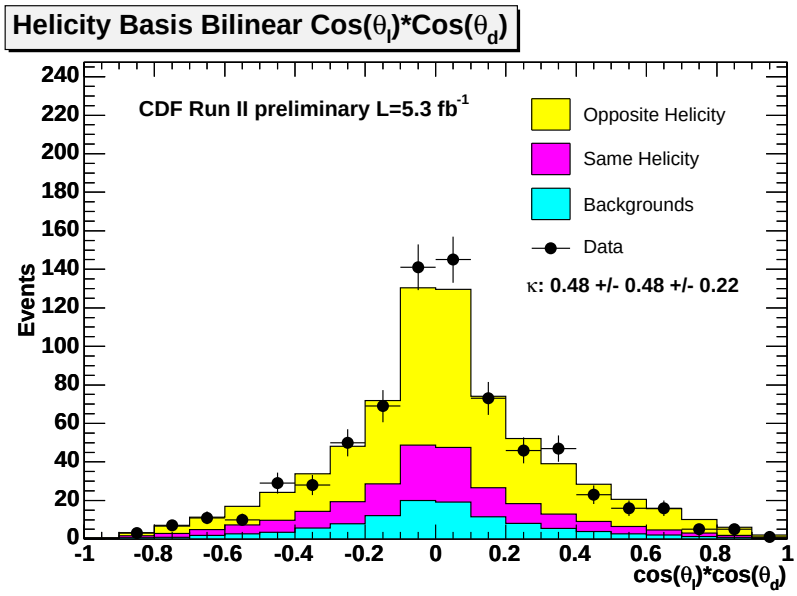

Figure 21: Helicity basis distribution of the $\cos(\theta_l)\cos(\theta_d))$ variable in data compared to the sum of our background model (light blue), the same helicity template (pink), and the opposite helicity template (yellow), where the opposite helicity fraction in the model is given by $F_{OH} = 0.74$.

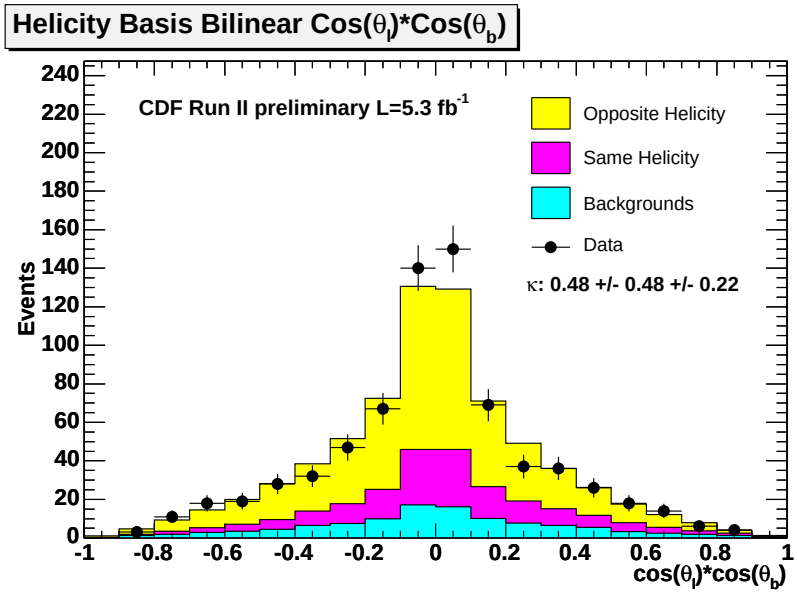

Figure 22: Helicity basis distribution of the $\cos(\theta_l)\cos(\theta_b))$ variable in data compared to the sum of our background model (light blue), the same helicity template (pink), and the opposite helicity template (yellow), where the opposite helicity fraction in the model is given by $F_{OH} = 0.74$.

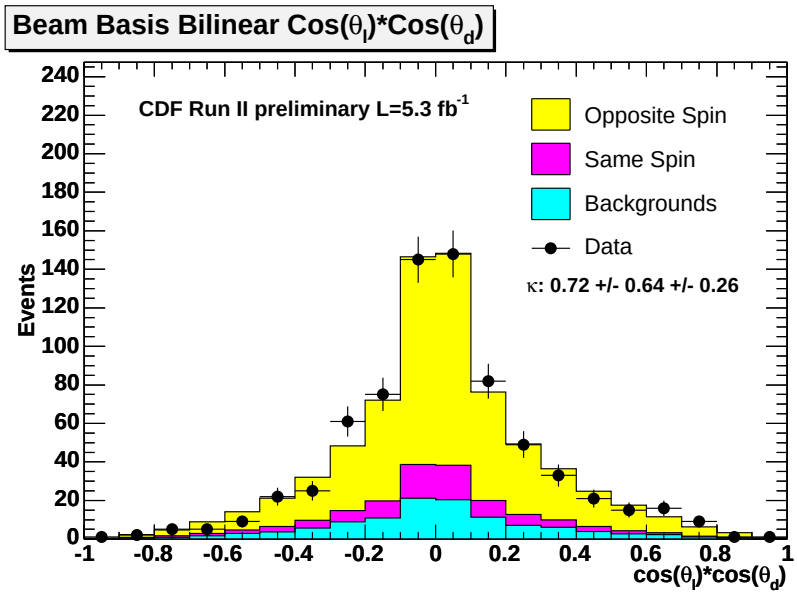

Figure 23: Beamline basis distribution of the $\cos(\theta_l)\cos(\theta_d))$ variable in data compared to the sum of our background model (light blue), the same spin template (pink), and the opposite spin template (yellow), where the opposite spin fraction in the model is given by $F_{OS} = 0.86$.

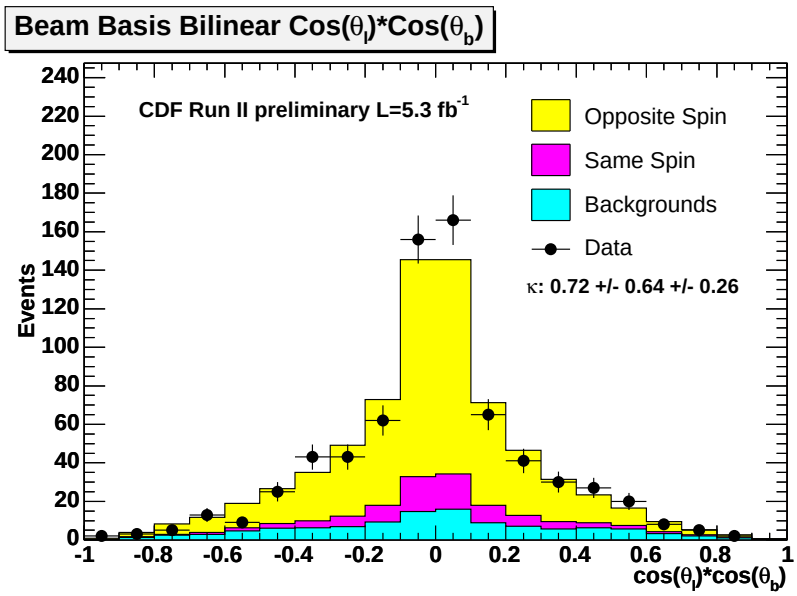

Figure 24: Beamline basis distribution of the $\cos(\theta_l)\cos(\theta_b))$ variable in data compared to the sum of our background model (light blue), the same spin template (pink), and the opposite spin template (yellow), where the opposite spin fraction in the model is given by $F_{OS} = 0.86$.

and National Science Foundation; the Italian Istituto Nazionale DP Fiske Nucleare; the Ministry of Education, Culture, Sports, Science and Technology of Japan; the Natural Sciences and Engineering Research Council of Canada; the National Science Council of the Republic of China; the Swiss National Science Foundation; the A.P. Sloan Foundation; the Bundesministerium f ur Bildung und Forschung, Germany; the Korean Science and Engineering Foundation and the Korean Research Foundation; the Particle Physics and Astronomy Research Council and the Royal Society, UK; the Institut National de Physique Nucleaire et Physique des Particules/CNRS; the Russian Foundation for Basic Research; the Comisi on Interministerial de Ciencia y Tecnolog a, Spain; the European Communitys Human Potential Programme; the Slovak R&D Agency; and the Academy of Finland.

References

[1] The CDF Collaboration, *http* : *//www−cdf.fnal.gov/cdfnotes/cdf*10048*_topspincorr_lepjet.pdf*, June 2009. 2

[2] G.L.Kane, G.A.Ladinsky, C.P.Yuan, Phys. Rev. D 45, 124 (1992). 2

[3] M. Arai, N. Okada, K. Smolek, V. Simak, arXiv:hep-ph/0701155, (2007). 2

[4] S. Willenbrock, Phys. Lett. B374, 169 (1996). 2

[5] G. Mahlon and S. parke, Phys. Rev. D 53, 4886 (1996). 2, 6, 8

[6] W. Bernreuther *et al.*, "Investigation of Top Quark Spin Correlations at Hadron Colliders", CERN-PH-TH-2004-206 (2004). 2

[7] The CDF Collaboration, *http* : *//www−cdf.fnal.gov/cdfnotes/cdf*9824*_spincorr*2.8*fb*− 1.*pdf*, June 2009. 2

[8] The CDF Collaboration, *http* : *//www−cdf.fnal.gov/cdfnotes/cdf*9724*_ttbarAfbMeasurement.pdf*, March 2009. 3